X-ray scattering from smectic films on a substrate

Dick K. G. de Boer
Philips Research Laboratories, Prof. Holstlaan 4, 5656 AA Eindhoven, The Netherlands
(Received 20 July 1998)

The combined effect of thermal fluctuations and substrate roughness replication in smectic liquid-crystalline films on a substrate is described. For that purpose a theory is developed which is an extension of existing continuum models. Both thermal fluctuations and roughness replication can be quantified in terms of the surface tension and the elastic constants for compression and bending of the smectic material. Model calculations show the effect of the various parameters. It is shown that the growth of roughness due to thermal fluctuations largely cancels the diminishment due to roughness replication. This explains why previous x-ray scattering measurements could be satisfactorily described in terms of fractal correlation functions. [S1063-651X(99)14802-5]

PACS number(s): 61.30.Cz, 61.30.Eb

I. INTRODUCTION

Smectic liquid crystals are materials characterized by one-dimensional ordering, that is, they exhibit layering [1]. Thin smectic films are technically interesting because of their optical, electrical, and adhesion properties, and they are of fundamental interest since they can serve as model systems in studying interactions in soft materials. X-ray scattering has been proven to be a powerful tool in studying smectic films. Specular scattering gives information on layering, whereas nonspecular (diffuse) scattering is very suitable to study fluctuations in the films. These techniques have been used to study free-standing films [2–5], as well as films on substrates prepared with the aid of the Langmuir-Blodgett technique [6–8] and of spin coating [9,10].

In general, the layers in smectic systems are not planar. This is not only because there are thermal fluctuations which destroy long-range order [1,4,11,12], but also because external disturbances propagate in the film [1]. In layers on substrates the latter results in replication of substrate roughness by the layered film. Figure 1 shows a schematic drawing of a smectic film on a substrate. Geer and co-workers [6–8] performed nonspecular x-ray measurements on such systems, and showed that their results cannot be explained by the effect of thermal fluctuations alone, but may be described in terms of fractal correlation functions [13]. Such correlation functions have been shown to yield a satisfactory description of polished substrates [13,14] and various inorganic multilayers [15,16], in which replication and deposition-based roughness are combined. However, there is no *a priori* reason why such a description should be applicable to smectic liquid-crystalline films.

In this paper we will develop a theory accounting for the effect of both thermal fluctuations and substrate roughness replication in smectic films. Our theory extends the existing theory for thermal fluctuations [4,11,12,17,18] to include the effect of propagation of roughness from the substrate. We will show that both effects can be explained in terms of the same three material parameters, viz., the surface tension and the elastic constants for compression and bending of the smectic layers.

Historically, three versions of the theory are known: a discrete version in which the displacement of the various layers is considered explicitly [11,12], a theory involving a continuous representation of the displacement field which has a finite number of modes determined by the interlayer distance [17] and a theory involving a continuous representation in which the number of modes is not limited from the beginning [4,18].

In Sec. II we will start by expanding the model of Poniewirski and Holyst [17] to include the effect of the substrate. Then, following Ref. [4], a shorter formulation of the end result will be introduced. Next we will describe how the x-ray scattering intensities can be calculated. In Sec. III examples will be given of calculations of the effect of roughness replication solely and in combination with thermal fluctuations. We will show that it is possible to explain published experimental results [8,16] in terms of the description presented here.

II. THEORY

We will consider a substrate with a smectic film consisting of N layers with a thickness d and a total thickness L

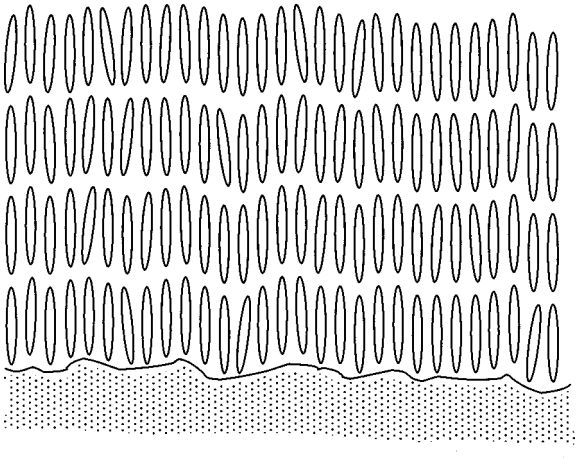

FIG. 1. Schematic representation of a smectic film on a substrate. The roughness of the smectic layers has two causes: replication of substrate roughness and thermal fluctuations.

$=Nd$. The layers can be displaced from their equilibrium positions in the direction perpendicular to the interfaces, which may be due to thermal fluctuations or to replication of substrate roughness. The displacement of (the middle of) a layer from its equilibrium position will be denoted by $u(\mathbf{x},z)$, with $\mathbf{x}=(x_1,x_2)$ and z being the coordinates parallel and perpendicular to the plane of the layers, respectively. We are interested in the correlation function $C(\mathbf{x},z,z')=\langle u(\mathbf{x},z)u(\mathbf{0},z')\rangle$, where $\langle\ \rangle$ indicates an ensemble average.

The free energy of the system may be expressed as [12]

$$F=\frac{1}{2}\int d^2\mathbf{x}\int_{-L/2}^{L/2}dz\left[B\left(\frac{\partial u(\mathbf{x},z)}{\partial z}\right)^2+K[\Delta_x u(\mathbf{x},z)]^2\right]+\frac{1}{2}\int d^2\mathbf{x}\left\{\gamma_+'\left[\nabla_{\mathbf{x}}u\left(\mathbf{x},\frac{1}{2}L\right)\right]^2+\gamma_-'\left[\nabla_{\mathbf{x}}u\left(\mathbf{x},-\frac{1}{2}L\right)\right]^2+K_{s+}\left[\Delta_{\mathbf{x}}u\left(\mathbf{x},\frac{1}{2}L\right)\right]^2+K_{s-}\left[\Delta_{\mathbf{x}}u\left(\mathbf{x},-\frac{1}{2}L\right)\right]^2\right\} \tag{1}$$

where B and K are the bulk elastic constants for compression and bending of the smectic layers, respectively; γ_+' and γ_-' are the surface tensions at the liquid-crystal–vapor ($z=L/2$) and liquid-crystal–substrate ($z=-L/2$) interfaces, respectively; and K_{s+} and K_{s-} are the surface elastic bending constants at these interfaces.

With the two-dimensional Fourier transform (FT) of $u(\mathbf{x},z)$,

$$u(\mathbf{q}_{\mathbf{x}},z)=\frac{1}{2\pi}\int d^2\mathbf{x}\exp(i\mathbf{q}_{\mathbf{x}}\cdot\mathbf{x})u(\mathbf{x},z),$$

where $\mathbf{q}_{\mathbf{x}}$ is the wave vector parallel to the layer plane, the free energy (1) can be written in the form $F=\Sigma_{\mathbf{q}_{\mathbf{x}}}F_{\mathbf{q}_{\mathbf{x}}}$. Furthermore, we will make use of the continuum-model description of Poniewirski and Holyst [17], writing $u(\mathbf{q}_{\mathbf{x}},z)=u_0(\mathbf{q}_{\mathbf{x}},z)+\delta u(\mathbf{q}_{\mathbf{x}},z)$, where $u_0(\mathbf{q}_{\mathbf{x}},z)$ is defined as the displacement minimizing $F_{\mathbf{q}_{\mathbf{x}}}$, which may be written as

$$u_0(\mathbf{q}_{\mathbf{x}},z)=p_+(\mathbf{q}_{\mathbf{x}},z)u_+(\mathbf{q}_{\mathbf{x}})+p_-(\mathbf{q}_{\mathbf{x}},z)u_-(\mathbf{q}_{\mathbf{x}}), \tag{2}$$

where $u_\pm(\mathbf{q}_{\mathbf{x}})=u(\mathbf{q}_{\mathbf{x}},\pm\frac{1}{2}L)$, and, with $\lambda=\sqrt{K/B}$,

$$p_\pm(\mathbf{q}_{\mathbf{x}},z)=\pm\sinh\left[\lambda q_x^2\left(z\pm\frac{1}{2}L\right)\right]\Big/\sinh(\lambda q_x^2 L). \tag{3}$$

Following Ref. [17], $\delta u(\mathbf{q}_{\mathbf{x}},z)$ can be expanded in a harmonic series $\delta u(\mathbf{q}_{\mathbf{x}},z)=\Sigma_{n=1}^{N-1}\delta u_n(\mathbf{q}_{\mathbf{x}})f_n(z)$, with $f_n(z)=\sqrt{2/L}\sin(n\pi z/L)$ for even n, and $f_n(z)=\sqrt{2/L}\cos(n\pi z/L)$ for odd n, yielding

$$F_{\mathbf{q}_{\mathbf{x}}}=\frac{1}{2}\sum_{n=1}^{N-1}\{[B(n\pi/L)^2+Kq_x^4][\delta u_n(\mathbf{q}_{\mathbf{x}})]^2\}+\frac{1}{2}q_x^2\left\{\gamma_+u_+(\mathbf{q}_{\mathbf{x}})^2+\gamma_-u_-(\mathbf{q}_{\mathbf{x}})^2+\frac{\sqrt{BK}}{\sinh(\lambda q_x^2L)}\{[u_+(\mathbf{q}_{\mathbf{x}})^2+u_-(\mathbf{q}_{\mathbf{x}})^2]\cosh(\lambda q_x^2L)-2u_+(\mathbf{q}_{\mathbf{x}})u_-(\mathbf{q}_{\mathbf{x}})\}\right\},$$

where we introduced $\gamma_\pm=\gamma_\pm'+K_{s\pm}q_x^2$. In most cases the q_x dependence of $\gamma_\pm$ is neglected. The values of $u_\pm(\mathbf{q}_{\mathbf{x}})$ have to be determined by the boundary conditions, which include the effects of both thermal fluctuations and replication of substrate roughness:

$$u_\pm(\mathbf{q}_{\mathbf{x}})=u_{t\pm}(\mathbf{q}_{\mathbf{x}})+u_{r\pm}(\mathbf{q}_{\mathbf{x}}).$$

We will assume that the thermal deviations $u_{t\pm}(\mathbf{q}_{\mathbf{x}})$ and the roughness deviations $u_{r\pm}(\mathbf{q}_{\mathbf{x}})$ fluctuate independently: $\langle u_{t\pm}(\mathbf{q}_{\mathbf{x}})u_{r\pm}(\mathbf{q}_{\mathbf{x}})\rangle=0$. This implies a separation of the correlation function in a part due to thermal fluctuations and a part due to roughness replication:

$$C(\mathbf{x},z,z')=C_t(\mathbf{x},z,z')+C_r(\mathbf{x},z,z').$$

The term $u_{r-}(\mathbf{q}_{\mathbf{x}})$ or, equivalently, its two-dimensional FT $u_{r-}(\mathbf{x})$, describes the substrate roughness. For instance, we can assume a fractal correlation function [13]

$$C_{r-}(\mathbf{x})=\langle u_{r-}(\mathbf{x})u_{r-}(\mathbf{0})\rangle=\sigma_-^2\exp[-(x/\xi)^{2H}], \tag{4}$$

where σ_-, ξ, and H are the root-mean-square (rms) roughness, the lateral correlation length, and the Hurst (or jaggedness) parameter of the substrate roughness, respectively. Furthermore, $u_{r+}(\mathbf{q}_{\mathbf{x}})$ has to be chosen in such a way that it minimizes $F_{\mathbf{q}_{\mathbf{x}}}$. This yields $u_{r+}(\mathbf{q}_{\mathbf{x}})=s(\mathbf{q}_{\mathbf{x}})u_{r-}(\mathbf{q}_{\mathbf{x}})$, with $s(\mathbf{q}_{\mathbf{x}})=1/[\nu_+\sinh(\lambda q_x^2L)+\cosh(\lambda q_x^2L)]$, where $\nu_\pm=\gamma_\pm/\sqrt{BK}$.

The terms in $F_{\mathbf{q}_{\mathbf{x}}}$ with $u_{t\pm}(\mathbf{q})$ contain cross terms. They can be written in diagonal form as

$$\frac{1}{2}\{A_1\langle[u_{t1}(\mathbf{q_x})]^2\rangle+A_1\langle[u_{t2}(\mathbf{q_x})]^2\rangle\},$$

where $u_{ti}(\mathbf{q_x})=\alpha_{i1}(\mathbf{q_x})u_{t+}(\mathbf{q_x})+\alpha_{i2}(\mathbf{q_x})u_{t-}(\mathbf{q_x})$, with $i=1$ and 2. It is easily shown that the eigenvalues are

$$A_{1,2}=\frac{1}{2}\sqrt{BK}q_x^2[\nu_++\nu_-+2\coth(\lambda q_x^2L) \pm\sqrt{(\nu_+-\nu_-)^2+4/\sinh^2(\lambda q_x^2L)}], \quad (5)$$

while the corresponding (orthonormal) eigenvectors are denoted by $[\alpha_{i1}(\mathbf{q_x}),\alpha_{i2}(\mathbf{q_x})]$, with $i=1$ and 2.

The $N-1$ values $\delta u_n(\mathbf{q_x})$ and the 2 values $u_{ti}(\mathbf{q_x})$ constitute the system's $N+1$ thermal eigenmodes with parallel wave vector $\mathbf{q_x}$, each corresponding with a free-energy content $\frac{1}{2}k_BT$. Hence

$$\langle[u_{ti}(\mathbf{q_x})]^2\rangle=k_BT/A_i$$

and

$$\langle[\delta u_n(\mathbf{q_x})]^2\rangle=k_BT/\{B[(n\pi/L)^2+\lambda^2q_x^4]\}.$$

With the above, Eq. (2) can be written as

$$u_0(\mathbf{q_x},z)=y(\mathbf{q_x},z)u_{r-}(\mathbf{q_x})+w_1(\mathbf{q_x},z)u_{t1}(\mathbf{q_x}) +w_2(\mathbf{q_x},z)u_{t2}(\mathbf{q_x}),$$

where

$$y(\mathbf{q_x},z)=p_+(\mathbf{q_x},z)s(\mathbf{q_x})+p_-(\mathbf{q_x},z)$$

and

$$w_j(\mathbf{q_x},z)=p_+(\mathbf{q_x},z)\alpha_{1j}^{-1}(\mathbf{q_x})+p_-(\mathbf{q_x},z)\alpha_{2j}^{-1}(\mathbf{q_x}), \quad (6)$$

where the matrix $\alpha_{ij}^{-1}(\mathbf{q_x})$ is the inverse of the matrix $\alpha_{ij}(\mathbf{q_x})$.

We will calculate $C(\mathbf{x},z,z')$ as the two-dimensional FT of the power spectral density $C(\mathbf{q_x},z,z')=\langle u(\mathbf{q_x},z)u(\mathbf{q_x},z')\rangle$. Since $u(\mathbf{q_x},z)$ has been written as a series of independent modes, we have

$$C(\mathbf{q_x},z,z')=\langle u_0(\mathbf{q_x},z)u_0(\mathbf{q_x},z')\rangle +\sum_{n=1}^{N-1}f_n(z)f_n(z')\langle[\delta u_n(\mathbf{q_x})]^2\rangle.$$

From what has been argued above, it follows that one can write

$$C(\mathbf{q_x},z,z')=C_t(\mathbf{q_x},z,z')+C_r(\mathbf{q_x},z,z'), \quad (7)$$

with

$$C_t(\mathbf{q_x},z,z')=k_BT\left[w_1(\mathbf{q_x},z)w_1(\mathbf{q_x},z')/A_1+w_2(\mathbf{q_x},z)w_2(\mathbf{q_x},z')/A_2+\frac{L}{B}\sum_{n=1}^{N-1}\frac{\cos(n\pi z_-/L)+(-1)^{n-1}\cos(n\pi z_+/L)}{n^2\pi^2+\lambda^2q_x^4L^2}\right], \quad (8)$$

$$C_r(\mathbf{q_x},z,z')=V(\mathbf{q_x},z,z')C_{r-}(\mathbf{q_x}), \quad (9)$$

where $z_+=z+z'$, $z_-=|z-z'|$. $C_{r-}(\mathbf{q_x})$ is the two-dimensional FT of $C_{r-}(\mathbf{x})$, and

$$V(\mathbf{q_x},z,z')=y(\mathbf{q_x},z)y(\mathbf{q_x},z')=\frac{\frac{1}{2}(1+\nu_+^2)\cosh[\lambda q_x^2(z_+-L)]+\frac{1}{2}(1-\nu_+^2)\cosh(\lambda q_x^2z_-)-\nu_+\sinh[\lambda q_x^2(z_+-L)]}{[\cosh(\lambda q_x^2L)+\nu_+\sinh(\lambda q_x^2L)]^2}. \quad (10)$$

Note that $V(\mathbf{q_x},z,z')$ expresses how the substrate roughness is replicated throughout the layer.

Following Mol *et al.* [4], the series in $C_t(\mathbf{q_x},z,z')$ can be calculated in the limit $N\to\infty$, yielding

$$C_t(\mathbf{q_x},z,z')=k_BT\left\{w_1(\mathbf{q_x},z)w_1(\mathbf{q_x},z')/A_1+w_2(\mathbf{q_x},z)w_2(\mathbf{q_x},z')/A_2+\frac{\cosh[\lambda q_x^2(L-z_-)]-\cosh(\lambda q_x^2z_+)}{2q_x^2\sqrt{BK}\sinh(\lambda q_x^2L)}\right\}. \quad (8')$$

The aforementioned authors [4] found that the results coincide with the result of the finite sum if z_- is assigned a minimum value $z_0=d/4$. We checked whether this also holds for our cases. We found that the results agree to within a few percent, except at the boundaries ($z=\pm L/2$) of the smectic film, where introduction of a cutoff for z_0 in Eq. (8′) may even yield negative numbers for high surface tension values [cf. Fig. 4(a)]. However, no problem occurs if the values calculated for the middle of a layer are assigned to the whole layer, and if we take $C_t(\mathbf{q_x},z,z')\geqslant 0$ at the substrate-film interface (i.e., for z or $z'=-L/2$). The result of Eq. (8′b) is equivalent to that derived in a different way by Shalaginov and Romanov [18].

The response of the smectic film is intrinsically isotropic in the $\mathbf{x}$ plane. If the substrate roughness is also isotropic, one can write

$$C(x,z,z')=\frac{1}{2\pi}\int_{q_{\min}}^{q_{\max}}q_x\,dq_xJ_0(q_xx)C(q_x,z,z'), \quad (11)$$

where J_0 denotes the Bessel function of order 0, $q_{\min}=2\pi/W$, and $q_{\max}=2\pi/a$, with W being the sample size and a the transverse molecule size. The rms roughness $\sigma(z)$ at depth z is given by $\sigma^2(z)=C(0,z,z)$. The differential cross section for diffuse x-ray scattering is given in the Born approximation [4,13] by

$$\frac{d\sigma}{d\Omega}=\frac{Sq_z^2}{16\pi^2}\sum_{n,k=0}^{N} r_n r_k^* \exp[iq_z(z_n-z_k)] \times\exp\left[-\frac{1}{2}q_z^2(\sigma_n^2+\sigma_k^2)\right]\int d^2\mathbf{x} \times\exp(i\mathbf{q_x}\cdot\mathbf{x})[\exp q_z^2 C_{nk}(\mathbf{x})-1], \quad (12)$$

where S is the detected irradiated sample surface area, q_z is the wave-vector transfer perpendicular to the layer plane, r_n is the Fresnel reflection coefficient [19] of layer n (which includes the effect of internal structure and may include the effect of local roughness [4]), $n=0$ denotes the substrate, z_n denotes the (equilibrium) position of the middle of layer n, $\sigma_n=\sigma(z_n)$ and $C_{nk}(\mathbf{x})=C(\mathbf{x},z_n,z_k)$.

The above formulas do not describe dynamical effects like enhanced scattering if either the incident or the detection angle is close to the critical angle for total reflection (''Yoneda wings'') [13]. The most pronounced effect is that of the film-vapor interface, which can be taken into account by multiplying the above formula by $|t_{\rm in}|^2|t_{\rm out}|^2$, where $t_{\rm in}$ and $t_{\rm out}$ are the Fresnel transmission coefficients of the top surface at the incident and detection angle, respectively [13]. This result can be obtained from a full treatment in the distorted-wave Born approximation [15,20,21] by taking into account only the effect of the top surface.

From the above expression [Eq. (12)] for the cross section, the diffusely scattered intensity can be calculated using Eqs. (3)–(11). In Sec. III we will discuss measurements involving a conventional diffractometer setup. Such equipment enables measurements in one direction, say x_1, using wide open slits in the perpendicular direction x_2. The measured intensity is then given by $I=I_0(2\Delta\theta/Sq_z)\int dq_{x_2}(d\sigma/d\Omega)$, where I_0 is the incident intensity and $\Delta\theta$ the divergence of the detector slit in the x_1 direction.

III. RESULTS AND DISCUSSION

A discussion of the properties of the thermal correlation function $C_t(x,z,z')$ can be found in Refs. [12] and [18]. A few more examples will be given below. For the calculation of $C_t(x,z,z')$ using Eq. (11), the effective sample size W (or, rather, the projected transverse x-ray coherence length [12]) and the transverse molecule size a have to be fixed. We took $W=2\times10^4$ mm and $a=0.4$ nm.

First we will discuss some properties of the correlation function $C_r(x,z,z')$ describing roughness replication. Figure 2 shows the results of calculations of the factor $V(\mathbf{q_x},z,z)$, Eq. (10), for various depths z. As discussed in Sec. II this quantity indicates to what extent roughness with a parallel wave vector $\mathbf{q_x}$ is replicated. It will be clear that roughness with low lateral frequencies is replicated better than that with high frequencies. The decay of $V(\mathbf{q_x},z,z)$ scales with the square root of λ and with the distance to the substrate. At large ν_+ values [Fig. 2(b)] the decay at low frequencies is faster than at small ν_+ [Fig. 2(a)]. We found that $V(\mathbf{q_x},z,z')$ is not very sensitive to the value of z_-.

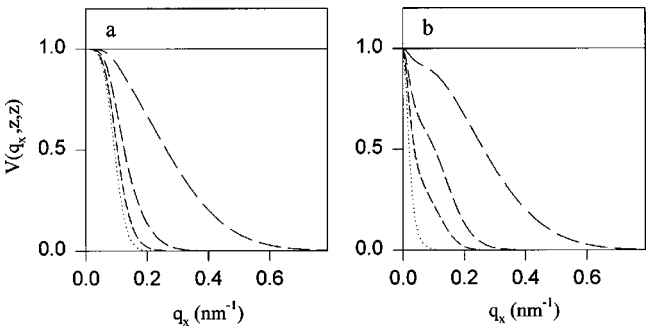

FIG. 2. Roughness replication factor $V(q_x,z,z)$ vs in-layer wave vector q_x at various depth values z. (a) $\nu_+=0$. (b) $\nu_+=10$. In all cases $L=100$ nm and $\lambda=1$ nm. From top to bottom: $z=-0.5L$ (horizontal solid line), $z=-0.45L$, $z=-0.25L$, $z=0$, and $z=0.5L$.

Figure 3 shows the corresponding correlation function $C_r(x,z,z)$, [Eq. (9)] for various depths z. Comparison of the various curves in one figure shows that the roughness decays as a function of the distance to the substrate. This decay is stronger at large ν_+ [Fig. 3(b)] than at small ν_+ [Fig. 3(a)], stronger at large λ [Fig. 3(a)] than at small λ [Fig. 3(c)], and stronger at large H [Fig. 3(a)] than at small H [Fig. 3(d)]. Furthermore, it can be seen that, at larger distances from the substrate, the weight shifts toward larger x values. This is a consequence of the fact that roughness with low lateral frequencies is replicated better than that with high frequencies.

In the next example several aspects of roughness replication combined with thermal fluctuations will be clarified. The

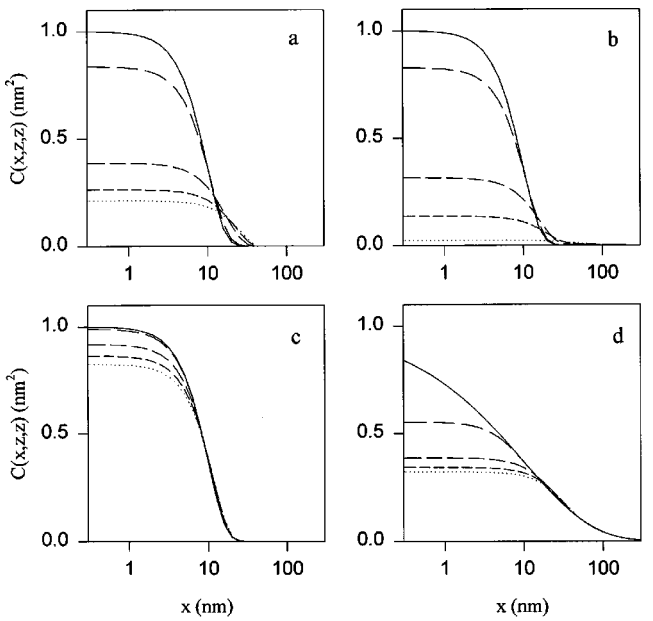

FIG. 3. Correlation function $C_r(x,z,z)$ vs in-layer distance x at various depth values z. (a) $\nu_+=0$, $\lambda=1$ nm, and $H=1$. (b) $\nu_+=10$, $\lambda=1$ nm, and $H=1$. (c) $\nu_+=0$, $\lambda=0.1$ nm, and $H=1$. (d) $\nu_+=0$, $\lambda=1$ nm, and $H=0.25$. In all cases $L=100$ nm, $\sigma_-=1$ nm, and $\xi=10$ nm. From top to bottom: $z=-0.5L$, $z=-0.45L$, $z=-0.25L$, $z=0$, and $z=0.5L$.

parameters used were taken from Geer *et al.* [8] for their sample $M1$, which is a film consisting of eight layers with a total thickness $L=32$ nm. They fitted their experimental data using the same (fractal) roughness parameters for all layers. We will only assume that the substrate roughness can be considered as fractal, and we will take values close to theirs as substrate roughness parameters: $\sigma_-=0.45$ nm, $\xi=50$ nm, and $H=0.35$. For the surface tension at the liquid-crystal–substrate interface we take $\gamma_-=\infty$. We found that the exact value of γ_- hardly affects the results, as long as ν_- is larger than 100. Furthermore we will take $T=300$ K and the values suggested [8] for the smectic film: $B=2.5\times10^8\,\mathrm{N\,m^{-2}}$, $K=10^{-11}$ N, and $\gamma_+=0.03\,\mathrm{N\,m^{-1}}$, resulting in $k_BT/\sqrt{BK}=0.08\,\mathrm{nm^2}$, $\lambda=0.2$ nm, $\nu_+=0.6$, and $\nu_-=\infty$.

Figure 4(a) shows the thermal contribution to the mean-square roughness σ^2 calculated using Eq. (8) (solid line) and the approximation (8b) (dashed line). As discussed in Sec. II, the values at the middle of the layers (dots), which are very close to those calculated using Eq. (8), will be used for the calculation of the x-ray scattering. At the substrate-film interface ($z=-16$ nm) Eq. (8) gives the correct answer $\sigma^2=0$ for $\gamma_-=\infty$, whereas Eq. (8′) yields a negative value. We will use the shorter expression (8′) below, but will take $\sigma^2=0$ if it results in a negative value.

Figure 4(b) again shows the thermal contribution (dashed), as well as the contribution due to replication of substrate roughness (dash-dotted) and the total roughness (solid line) as the sum of the two. The thick dots indicate the values that will be used for the scattering calculation. As in Fig. 3, the roughness due to roughness replication (dash-dotted line) decays with the distance to the substrate. This decay is slow because of the small values of λ and ν_+. The thermal roughness (dashed line), on the other hand, grows with that distance. The sum of the two (solid line) remains remarkably constant. This is the case with the assumed parameters of the smectic film. If λ or ν_+ is larger, or if $k_BT/\sqrt{BK}$ is smaller, the decay of σ^2 with z is faster. The behavior with $\nu_+=6$ (dotted line) is shown as an example.

Figure 4(c) shows the power spectral density $C(q_x,z,z)$. The top (solid) line shows the fractal behavior of the substrate roughness. The top layer has a contribution due to roughness replication that decays much faster at high spatial frequencies (medium-long dashes), having a value below $10^{-3}\,\mathrm{nm^4}$ at $q_x=1\,\mathrm{nm^{-1}}$. The thermal contribution to the top-layer roughness (short dashes) is slightly below 1 $\mathrm{nm^4}$ at low frequencies, but decays much more slowly than that due to roughness replication. The sum of the two (long dashes) is close to the power spectral density of the substrate up to frequencies somewhat above 1 $\mathrm{nm^{-1}}$. In the $\nu_+=6$ case (dotted line) the deviation from the substrate power spectral density starts at much lower frequencies, but at higher frequencies the thermal contribution partly compensates for this. The interlayer correlation functions (not shown) were also found to be close to the substrate's correlation function.

Figure 4(d) shows the Fourier transform of Fig. 4(c), i.e., the roughness correlation function $C(x,z,z)$. It exhibits the same trend as Fig. 4(c), with the differences mainly at small values of x.

As examples of x-ray scattering calculations, Figs 4(e) and 4(f) show rocking curves (transverse scans) obtained with the detector angle at the values for the first and second

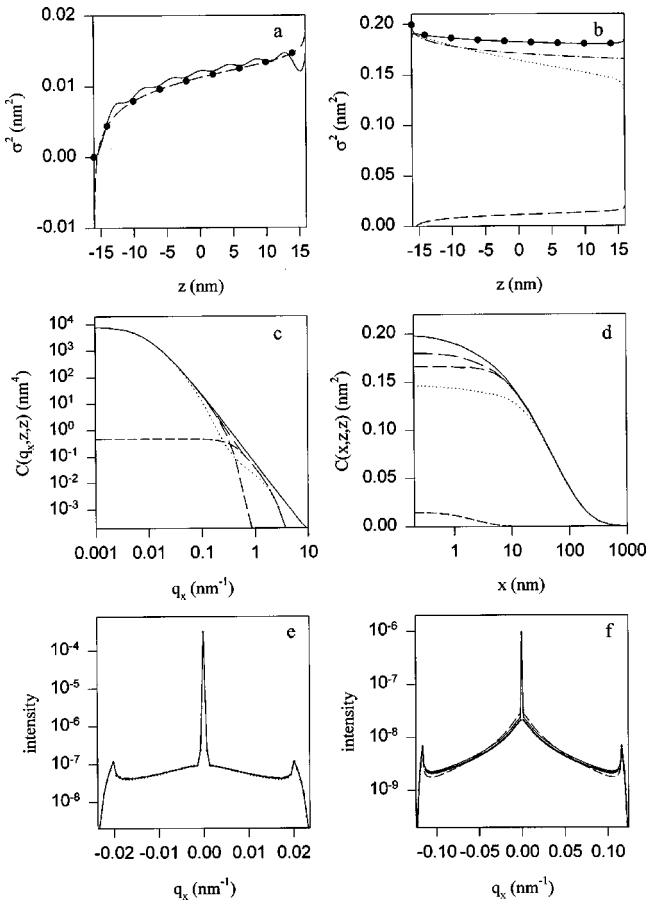

FIG. 4. Results of calculations for a smectic film of eight layers on a substrate. $L=32$ nm, $\lambda=0.2$ nm, $\nu_+=0.6$, $\nu_-=\infty$, $k_BT/\sqrt{BK}=0.08\,\mathrm{nm^2}$, $\sigma_-=0.45$ nm, $\xi=50$ nm, and $H=0.35$. (a) and (b): Mean-square roughness $\sigma^2(z)$ vs depth. (a) Thermal contribution only. Solid line: using Eq. (8); dashed line: using Eq. (8′); thick dots: values used to calculate diffuse scattering. (b) Dashed line: thermal contribution [dashed line from Fig. (4a)]; dash-dotted line: roughness replication; solid line: total roughness; thick dots: values used to calculate diffuse scattering; dotted line: calculated using $\nu_+=6$. (c) Power spectral density $C(q_x,z,z)$ vs in-layer wave vector q_x. (d) Correlation function $C(x,z,z)$ vs in-layer distance x. (c) and (d): From top to bottom: substrate roughness (solid line), total roughness of the top layer (long dashes), roughness of the top layer due to roughness replication (medium-long dashes), thermal fluctuations of the top layer (short dashes); dotted line: calculated using $\nu_+=6$. (e) and (f): rocking curves (scattered intensity vs in-layer wave vector q_x, using Cu $K\alpha$ radiation). Dots: calculated with values found in Ref. [8] to fit experiments; solid line: calculated with the above values; dashed line: calculated using $\nu_+=6$; (e) rocking curve at first Bragg peak; (f) rocking curve at second Bragg peak.

Bragg peaks (which are due to the layer periodicity [8,10]), respectively. The solid lines were calculated using the above parameters. The dots mimic the experimental data, which were calculated using the parameters found in Ref. [8]; that is, the same fractal roughness throughout the film. Interestingly, the parameters used for the smectic film yield curves that are hardly distinguishable from those calculated with the fractal model. This is certainly true for small λ and ν_+ values, but we found that this remains the case for a large range of parameters. For example, when different values for the

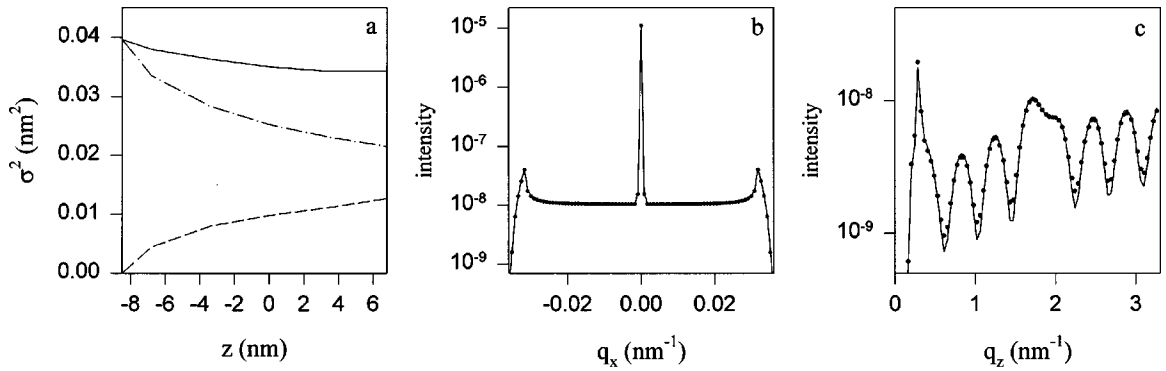

FIG. 5. Results of calculations for a smectic film of five layers on a substrate. $L=17$ nm, $\lambda=0.2$ nm, $\nu_+=0.6$, $\nu_-=\infty$, $k_BT/\sqrt{BK}=0.08$ nm^2, $\sigma_-=0.2$ nm, $\xi=5$ nm, and $H=0.75$. (a) Mean-square roughness $\sigma^2(z)$ vs depth. Dashed line: thermal contribution; dash-dotted line: roughness replication; solid line: total roughness. (b) and (c) Diffuse scattering intensity (using Cu $K\alpha$ radiation). Dots: calculated with values found in Ref. [16] to fit experiments; solid line: calculated with the above values. (b) Rocking curve (scattered intensity vs in-layer wave vector q_x) at first Bragg peak. (c) Offset scan (scattered intensity vs perpendicular wave vector q_z) at an offset angle of 1 mrad.

smectic-film parameters are used (dashed lines: $\nu_+=6$), the data are not distinguishable in a measurement for a small q_x range [Fig. 4(e)], though they may be distinguished if a larger q_x range can be reached [Fig. 4(f)].

A way of distinguishing more accurately between the various models is suggested in Fig. 4(c). If a measurement can be done over a large q_x range and no integration over the perpendicular direction is performed, a deviation from fractal behavior is expected at large q_x values. A large parallel wave-vector range will be available if a surface-diffraction setup is used in which the x-ray beam is collimated in two directions [5]. The required large dynamic range is attainable with synchrotron radiation.

We found that the other results of Ref. [8], in which the measurements were fitted using the same (fractal) model, can be explained in the same way. Here too, substrate roughness replication results in curves which start to deviate from fractal, whereas the addition of thermal fluctuations brings the total close to the substrate correlation function again.

As a final example we will consider our own recent measurements [16] of a spin-coated smectic film, which we interpreted with a similar model. We used the expression $C_{nk}(\mathbf{x})=\sqrt{C_{nn}(\mathbf{x})C_{kk}(\mathbf{x})}\exp(-|z_n-z_k|/\xi_\perp)$, where a form like Eq. (4) was used for $C_{nn}(\mathbf{x})$, and $\xi_\perp$ is a perpendicular correlation length. [The model of Ref. [8] can be regarded as this model with a perfect perpendicular correlation, that is, $C_{nn}(\mathbf{x})=C_{kk}(\mathbf{x})$ and $\xi_\perp=\infty$.] We found [10] that the sample had a very rough top layer, containing holes. For simplicity we will omit that effect in the present analysis. We will describe only the effect of the inner interfaces, the contribution of which could be fitted by taking $\xi_\perp=5$ nm and $\sigma=2$ nm, $\xi=50$ nm, and $H=0.75$ for all interfaces. We applied our present model to this material by using the latter three parameters for the substrate, and the same parameters for the smectic film as in the previous example. Figure 5 shows the results of the calculations. In Fig. 5(a) it can be seen that, here too, substrate roughness replication results in a decrease in roughness in the case of layers further from the substrate (dash-dotted line), whereas the total roughness, including thermal fluctuations (dashed line), remains very constant (solid line).

Figures 5(b) and 5(c) show the results of diffuse scattering calculations. Again the rocking curve around the first Bragg peak [Fig. 5(b), solid line] is not distinguishable from that calculated with the fractal model (dots). Hardly any difference is seen in an offset scan either [Fig. 5(c)]. The peak just before 2 nm^{-1} is the first Bragg peak, which is broadened because the perpendicular correlation is not perfect. It will be difficult to obtain data of sufficient quality to distinguish between the models, but again measurements in a surface-diffraction setup will give more detailed information.

IV. CONCLUSION

We have presented a theory for the combined effect of roughness replication and thermal fluctuations in smectic films on a substrate. Three material parameters are needed to describe the effect: the surface tension (γ_+) and the elastic constants for compression (B) and bending (K) of the smectic layers.

It was found that roughness due to replication of substrate roughness decays with the distance to the substrate, whereas that due to thermal fluctuations increases. In general, the decay due to roughness replication is small because of the strong effect of the substrate boundary and the smectic stiffness. Even when this decay is large enough to be detected, the opposite effect of thermal fluctuations largely compensates for this effect. If a fractal correlation function is assumed for the substrate, as is usual for polished surfaces, the resulting roughness correlation function for the smectic layers is also found to be very close to fractal. Moreover, the limited in-layer wave-vector range in a conventional diffraction experiment hampers the observation of deviations from fractal behavior.

We conclude that the above-mentioned smectic material parameters cannot be determined in a very accurate way via measurements of thin films on a substrate using a conventional diffractometer setup. The use of a surface-diffraction setup is more promising because of its large parallel wave-vector range.

ACKNOWLEDGMENT

Discussions with Professor W. H. de Jeu have been stimulating to perform this work.

[1] P. G. de Gennes, *The Physics of Liquid Crystals* (Clarendon, Oxford, 1974).
[2] S. Gierlotka, P. Lambooy, and W. H. de Jeu, Europhys. Lett. **12**, 341 (1990).
[3] D. J. Tweet, R. Holyst, B. D. Swanson, H. Stragier, and L. B. Sorensen, Phys. Rev. Lett. **65**, 2157 (1990).
[4] E. A. L. Mol, J. D. Shindler, A. N. Shalaginov, and W. H. de Jeu, Phys. Rev. E **54**, 536 (1996).
[5] E. A. L. Mol, G. C. L. Wong, J. M. Petit, F. Rieutord, and W. H. de Jeu, Phys. Rev. Lett. **79**, 3439 (1997).
[6] R. E. Geer, R. Shashidar, A. F. Thibodeaux, and R. S. Duran, Phys. Rev. Lett. **71**, 1391 (1993).
[7] R. E. Geer and R. Shashidar, Phys. Rev. E **51**, R8 (1995).
[8] R. E. Geer, S. B. Qadri, R. Shashidar, A. F. Thibodeaux, and R. S. Duran, Phys. Rev. E **52**, 671 (1995).
[9] G. Henn, M. Stamm, H. Poths, M. Rücker, and J. Rabe, Physica B **221**, 174 (1996).
[10] M. W. J. van der Wielen, M. A. Cohen Stuart, G. J. Fleer, D. K. G. de Boer, A. J. G. Leenaers, R. P. Nieuwhof, A. T. M. Marcelis, and E. J. R. Sudhölter, Langmuir **13**, 4762 (1997).
[11] R. Holyst, D. J. Tweet, and L. B. Sorensen, Phys. Rev. Lett. **65**, 2153 (1990).
[12] R. Holyst, Phys. Rev. A **44**, 3692 (1991).
[13] S. K. Sinha, E. B. Sirota, S. Garoff, and H. B. Stanley, Phys. Rev. B **38**, 2297 (1988).
[14] C. Teichert, J. F. MacKay, D. E. Savage, M. G. Lagally, M. Brohl, and P. Wagner, Appl. Phys. Lett. **66**, 2346 (1995).
[15] V. Holý, J. Kubena, I. Ohlídal, K. Lischka, and W. Plotz, Phys. Rev. B **47**, 15 896 (1993).
[16] D. K. G. de Boer, A. J. G. Leenaers, M. W. J. van der Wielen, M. A. Cohen Stuart, G. J. Fleer, R. P. Nieuwhof, A. T. M. Marcelis, and E. J. R. Sudhölter, Physica B **248**, 274 (1998).
[17] A. Poniewirski and R. Holyst, Phys. Rev. B **47**, 9840 (1993).
[18] A. N. Shalaginov and V. P. Romanov, Phys. Rev. E **48**, 1073 (1993).
[19] L. G. Parratt, Phys. Rev. **95**, 359 (1954).
[20] J. Daillant and O. Bélorgey, J. Chem. Phys. **97**, 5824 (1992).
[21] D. K. G. de Boer, Phys. Rev. B **53**, 6048 (1996).